Molecular dynamics methods for bioelectronic systems in photosynthesis

Ioan Kosztin

Department of Physics & Astronomy, University of Missouri, Columbia, MO 65211, USA

Klaus Schulten

Beckman Institute and Department of Physics,

University of Illinois, Urbana, IL 61801, USA

(Dated: May 16, 2006)

I. INTRODUCTION

Photosynthetic systems contain a variety of large photoactive *pigment-protein complexes* (PPCs) that carry out important functions necessary for maintaining the life cycle of photosynthetic organisms (e.g., light-harvesting, quinone redox reactions and ATP synthesis). Being involved in electron and electronic excitation transfer processes PPCs have been the subject of numerous experimental and theoretical studies [1].

In PPCs the photoactive pigment molecules are held in well defined spatial configuration and orientation by a scaffold of proteins. At physiological temperature the dynamics of the protein matrix are governed mainly by classical physics and, therefore, can be studied by means of molecular dynamics (MD) simulations provided that a sufficiently high resolution molecular structure of the system is available. However, key to photosynthesis is the interaction of light with the electronic degrees of freedom of the pigment molecules which is quantum mechanical in nature. In general, the properties of PPCs are determined by the chemical nature of the pigment, the electronic interactions between the pigment molecules, and the interactions between pigment molecules and their environment (e.g., protein, lipid and solvent molecules). In photosynthetic organisms PPCs function at physiological temperature and, therefore, their electronic and optical properties are strongly affected by thermal fluctuations which represent the main source of dynamic disorder in these systems. Thus, the theoretical description of thermally disordered PPCs is a complicated stochastic quantum mechanics problem that requires to determine and characterize the quantum states of the interacting pigment molecules in the presence of a fluctuating environment. Even in the simplest theoretical models of PPCs the simultaneous treatment of the electronic coupling between the pigments and the effect of thermal disorder can be done only approximately [2–5]. Most of the currently used theoretical approaches for calculating the electronic transfer rates and optical spectra of PPCs are based on empirical stochastic models in which several fitting parameters are adjusted to simulate the corresponding experimental results [6].

In this chapter a general approach for predicting and characterizing charge transfer, spectral and optical properties, e.g., linear absorption (OD) and circular dichroism (CD) spectra, of PPCs is presented [7, 8]. The approach that combines MD simulations, quantum chemistry (QC) calculations and quantum many-body theory is based solely on atomic-level crystal structure information. The conformational dynamics of the protein matrix embedded into its natural environment (a fully solvated lipid bilayer) are followed by means of classical MD simulations. Next, for each pigment molecule, modeled as a quantum two level system, the energy gap (and, in case of optical spectra, the transition dipole moment) time series are determined along a properly chosen segment of the MD trajectory by means of QC calculations. Finally, the transfer rate and/or optical spectra are determined in terms of a *lineshape function* which, within the cumulant approximation, can be calculated from the sole knowledge of the energy gap time series. The authors made every effort to present the material in a manner that is accessible to the general biophysics readership, including both theorists and experimentalists.

The chapter is organized as follows. In the first part the theoretical background of the combined MD/QC method for calculating optical spectra and electron transfer rates is presented by following the same general strategy. The relationship of the presented method to the polaron model and spin-boson model calculations

is also clarified. To make the presentation self contained, a brief description of the considered model systems, i.e., the light harvesting complex LH2 from *Rs. molischianum* (for calculting OD and CD spectra), and the photosynthetic reaction center from *Rb. sphaeroides* (for calculating electron transfer rates) is provided. In the second part of the chapter the presented theory is demonstrated by calculating the optical spectra of the LH2 and the electron transfer rate in the reaction center.

II. OPTICAL TRANSITIONS AT FINITE TEMPERATURE

Following their crystal structure determination, LH2 complexes from *Rs. molischianum* [10] and *Rsp. acidophila* [11] have been extensively studied both experimentally [12–19] and theoretically [7, 14, 17, 19–26]. LH2 from *Rs. molischianum* (Fig. 1) is an octamer of $\alpha\beta$-heterodimers arranged in a ring-like structure [27, 28]. Each protomer consists of an α- and a β-apoprotein which binds non-covalently one BChl-a molecule that absorbs at 800 nm (referred to as B800), two BChl-a molecules that absorb at 850 nm (referred to as B850) and at least one carotenoid that absorbs around 500 nm. The total of 16 B850 and 8 B800 BChls form two circular aggregates, both oriented parallel to the surface of the membrane. The excitonic coupling between the B800s is negligible because of their large spatial separation (~ 22 Å). Therefore, the optically active Q_y excited electronic states of the B800s are almost degenerate. On the other hand, the tightly packed B850s (with and average Mg$-$Mg distance of ~ 9.2 Å within the $\alpha\beta-$heterodimer and ~ 8.9 Å between the neighboring protomers) are strongly coupled and the corresponding Q_y excited states form an excitonic band in which the states that carry most of the oscillator strength are clustered about ~ 850 nm (1.46 eV). Another important difference between the two BChl rings is that while the B800s are surrounded by mostly hydrophilic protein residues the binding pocket of the B850s is predominantly hydrophobic [10]. Thus, although both B800s and B850s are chemically identical BChl molecules their specific spatial arrangement and the nature of their protein environment shape differently their spectral and optical properties. For example, it is quite surprising that the two peaks, due to the B800 and B850 BChls, in the experimental OD spectrum of LH2 from *Rs. molischianum* at room temperature [22, 30] have comparable widths although, as mentioned above, the B800 levels are almost degenerate while the B850 levels form a ~ 0.2 eV wide excitonic band.

In order to calculate the linear optical absorption of a PPC one assumes that the electronic properties of individual pigment molecules can be described in terms of a two-level system, formed by the ground state and the lowest excited singlet state (e.g., the Q_y state in the case of BChl) involved in the optical absorption process. Neglecting for the moment the direct interaction between the pigments (e.g., by assuming a sufficiently large spatial separation between them as in the case of the B800s in LH2), one denotes these

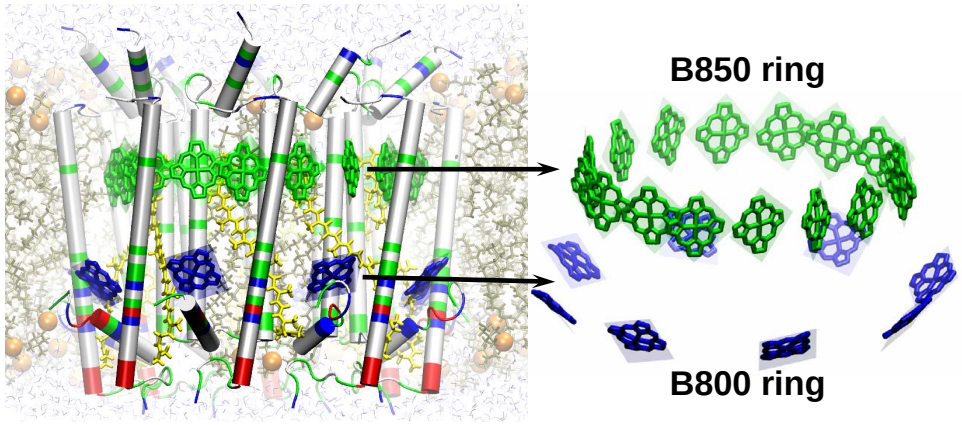

FIG. 1: **Left:** Side view of the LH2 complex from *Rs. molischianum* (entry code 1LGH in Protein Data Bank) embeded in a fully solvated POPC lipid bilayer. The transmembrane helices of the apoprotein subunits are shown as cylinders (cartoon representation) and are colored by residue type; dark (light) colors represent hydrophilic (hydrophobic) residues. For clarity only the BChl macrocycles and the back half of the lipids are shown. The clearly visible B800 (B850) ring is surrounded mostly by polar and charged (nonpolar) protein residues. **Right:** Tilted side view of the quantum system formed by the optically active B800 and B850 rings. Graphics rendered with the program VMD [29].

two states for pigment $n = 1,\ldots N$, as $|0\rangle \equiv |0_n\rangle$ and $|n\rangle \equiv |1_n\rangle$, respectively. Once the interaction between the pigment and its environment composed of the protein matrix, lipid membrane and solvent molecules is taken into account these two levels transform into still well separated energy bands $|0;\lambda_0\rangle = |0\rangle|\lambda_0\rangle$ and $|n;\lambda_n\rangle = |n\rangle|\lambda_n\rangle$. Here the quantum numbers λ_0 and λ_n specify the state of the n^{th} pigment on the ground- and excited-state potential energy surface, respectively. Because the exact quantum mechanical treatment of the eigenstates $|0;\lambda_0\rangle$, $|n;\lambda_n\rangle$ and of the corresponding energy eigenvalues $\mathscr{E}_{0,\lambda_0}$, $\mathscr{E}_{n,\lambda_n}$ is out of question, usually the quantum numbers λ_0 and λ_n are associated with the vibronic states of the PPC that can be modeled within the harmonic approximation as a phonon heat bath. An alternative approach is to follow the dynamics of the nuclear degrees of freedom of the PPC by all-atom MD simulations, and determine the energy gap time series $\Delta E_n(t) = \mathscr{E}_n(t) - \mathscr{E}_0(t)$ at each MD time step by means of QC calculations. The main assumption of this approach is that the obtained energy gap time series $\Delta E_n(t)$ can be used to calculate approximately equilibrium quantities (such as energy gap density of states and time autocorrelation functions) of the original system without the knowledge of the exact energy gap spectrum $\Delta\mathscr{E}_{n,\lambda_n,\lambda_0} = \mathscr{E}_{n,\lambda_n} - \mathscr{E}_{0,\lambda_0}$.

In the absence of the excitonic coupling between the pigment molecules, the Hamiltonian of the system can be written as $\mathscr{H} = H_0 + H$, where

$$H_0 = \sum_{\lambda_0} |0;\lambda_0\rangle \mathscr{E}_{0,\lambda_0} \langle 0;\lambda_0|, \tag{1}$$

and

$$H = \sum_n H_n = \sum_{\lambda_n} |n;\lambda_n\rangle \mathscr{E}_{n,\lambda_n} \langle n;\lambda_n| \,. \tag{2}$$

The electric dipole moment operator through which the incident light field couples to the n^{th} pigment molecule is given by

$$\hat{\boldsymbol{\mu}}_n = \sum_{\lambda_n,\lambda_0} \mathbf{d}_{n,\lambda_n,\lambda_0} |n;\lambda_n\rangle\langle 0;\lambda_0|, \tag{3}$$

where the transition dipole moment (TDM) matrix element $\mathbf{d}_{n,\lambda_n,\lambda_0}$ in the Condon approximation [3] can be written

$$\mathbf{d}_{n,\lambda_n,\lambda_0} \approx \mathbf{d}_n \langle \lambda_n|\lambda_0\rangle. \tag{4}$$

Here $\mathbf{d}_n = \langle 1|\hat{\boldsymbol{\mu}}_n|0\rangle$ is the real TDM vector whose time series can be determined from the same combined MD/QC calculations as $\Delta E_n(t)$. Note that while $\langle 1|0\rangle = 0$, in general the Franck-Condon factors $\langle \lambda_n|\lambda_0\rangle$ are finite [3].

A. Linear absorption and lineshape function

Because, in general, the wavelength of the incident light is much larger than the size of PPCs, in leading approximation, the electric component of the light field can be regarded as being uniform throughout the system. Thus, according to standard linear response theory, the corresponding OD spectrum $I(\omega)$ is proportional to the dipole-dipole correlation function [3, 4]

$$I(\omega) \propto \omega \sum_{n,m} \mathrm{Re}\left[\int_0^\infty dt e^{i\omega t} \left\langle \hat{\mu}^\dagger_{m,i}(0)\hat{\mu}_{n,i}(t)\right\rangle\right], \tag{5}$$

where $\hat{\mu}_{n,i}(t) = e^{-iHt}\hat{\mu}_{n,i}(0)e^{iH_0t}$ is the $i \in \{x,y,z\}$ component of the time dependent electric dipole operator, and $\langle \ldots\rangle = \mathrm{Tr}\left\{Z_0^{-1}\exp(-\beta H_0)\ldots\right\}$ with $\beta = 1/k_BT$ the usual temperature factor and Z_0 the corresponding partition function. To simplify notation, throughout this paper we use units in which $\hbar = 1$, and apply the convention of implicit summation over repeated indices. By employing Eqs. (1),(2) and (3), the quantum dipole correlation function in Eq. (5) can be expressed as

$$\left\langle \hat{\mu}^\dagger_{m,j}(0)\hat{\mu}_{n,i}(t)\right\rangle = d_{n,i}d_{m,j}\delta_{nm}\left\langle e^{iH_0t}e^{-iH_nt}\right\rangle, \tag{6}$$

where δ_{nm} is the usual Kronecker delta symbol. With Eq. (6) the OD spectrum of an aggregate of noninteracting pigments in their native environment can be written in terms of the *lineshape function*

$$A_n(\omega) \equiv \mathrm{Re}\int_0^\infty dt e^{i\omega t}\left\langle e^{iH_0t}e^{-iH_nt}\right\rangle \tag{7}$$

as

$$I(\omega) \propto \omega \sum_n d_n^2 A_n(\omega). \tag{8}$$

The main difficulty in calculating the quantum time correlation function in Eq. (7) is due to the fact that the Hamiltonians H_0 and H_n do not commute. If they would, then the lineshape function could be expressed in terms of the energy gap density of states (DOS). Indeed, in this case $\left\langle e^{iH_0 t} e^{-iH_n t} \right\rangle \approx \langle \exp(-i\Delta H_n t) \rangle$, with $\Delta H_n = H_n - H_0$, and by calculating the time integral in Eq. (7) would follow

$$A_n(\omega) \approx \pi \mathscr{N}(\omega) \,, \tag{9}$$

$$\mathscr{N}(\omega) \equiv \langle \delta(\omega - \Delta H_n) \rangle \approx \langle \delta(\omega - \Delta E_n(t)) \rangle, \tag{10}$$

where the density of states $\mathscr{N}(\omega)$ is approximated by the binned histogram of the energy gap fluctuations $\Delta E_n(t)$ obtained from combined MD/QC calculations [7–9]. In general, Eqs. (9)-(10) overestimate the broadening of the lineshape function. Indeed, the Fourier transform of the exact spectral representation of the correlation function

$$\left\langle e^{-iH_0 t} e^{iHt} \right\rangle = \sum_{\lambda_0, \lambda_n} \rho_{\lambda_0} |\langle \lambda_0 | \lambda_n \rangle|^2 e^{-i(\mathscr{E}_{n,\lambda_n} - \mathscr{E}_{0,\lambda_0})t} \,, \tag{11}$$

where $\rho_{\lambda_0} = Z_0^{-1} exp(-\beta \mathscr{E}_{0,\lambda_0})$ is the statistical matrix of the electronic ground state, yields

$$A(\omega) = 2\pi \sum_{\lambda_0, \lambda_n} \rho_{\lambda_0} |\langle \lambda_0 | \lambda_n \rangle|^2 \delta(\omega - \Delta \mathscr{E}_{n,\lambda_n,\lambda_0}) \,, \tag{12}$$

which can be regarded as a Franck-Condon weighted and thermally averaged density of state[31]. By setting the Franck-Condon factors $\langle \lambda_0 | \lambda_n \rangle$ equal to unity in (12) one obtains Eqs. (9)-(10). Since it is not possible to determine all these factors, it is often convenient to use Eqs. (9)-(10) as a rough estimate of $A_n(\omega)$ for calculating the OD spectrum.

A systematic way of calculating the correlation function in (7) is the cumulant expansion method [3, 32, 33]. Within the second order cumulant approximation that is often used in optical spectra calculations[4] one has

$$\begin{aligned} \left\langle e^{iH_0 t} e^{-iH_n t} \right\rangle &= \left\langle \mathrm{T} \, \exp\left[-i \int_0^t d\tau \Delta H_n(\tau) \right] \right\rangle \\ &\approx \exp\left[-i \langle \Delta H_n \rangle t - \int_0^t d\tau (t - \tau) \mathscr{C}_n(\tau) \right], \end{aligned} \tag{13}$$

where T is the time ordering operator, $\Delta H_n(t) = e^{iH_0 t} \Delta H_n e^{-iH_0 t}$, $\mathscr{C}_n(t) = \langle \delta H_n(t) \delta H_n(0) \rangle$, and $\delta H_n(t) = \Delta H_n(t) - \langle \Delta H_n \rangle$. The quantum statistical averages in Eq. (13) can be be approximated by the corresponding classical ones, involving the energy gap time series $\Delta E_n(t)$, as follows

$$\langle \Delta H_n \rangle \approx \langle \Delta E_n(t) \rangle \equiv \omega_n, \tag{14}$$

$$\mathrm{Re}[\mathscr{C}_n(t)] \approx C_n(t) \equiv \langle \delta E_n(t) \delta E_n(0) \rangle \,, \tag{15}$$

where $\delta E_n(t) = \Delta E_n(t) - \langle \Delta E_n \rangle$. It should be noted that although the approximation of the real part of a quantum time correlation function by the corresponding classical correlation function as in Eq. (15) is generally accepted [9, 34, 35], other approximation schemes have also be used and tested [36].

Next, by invoking the *fluctuation dissipation theorem* [4], $\widetilde{\mathscr{C}}_n(-\omega) = \exp(-\beta\omega)\widetilde{\mathscr{C}}_n(\omega)$, where $\widetilde{\mathscr{C}}_n(\omega) = \int_{-\infty}^{\infty} dt\, \mathscr{C}_n(t) \exp(i\omega t)$ is the Fourier transform of $\mathscr{C}_n(t)$, the quantum correlation function in terms of the real *spectral density*

$$J_n(\omega) = \frac{1}{2}\left[\widetilde{\mathscr{C}}_n(\omega) - \widetilde{\mathscr{C}}_n(-\omega)\right] = \frac{1}{2}\left(1 - e^{-\beta\omega}\right)\widetilde{\mathscr{C}}_n(\omega) \tag{16}$$

can be written as

$$\begin{aligned} \mathscr{C}_n(t) &= \mathscr{C}_n'(t) - i\mathscr{C}_n''(t) \\ &= \int_0^{\infty} \frac{d\omega}{\pi} J_n(\omega) \left[\coth(\beta\omega/2)\cos\omega t - i \sin\omega t\right] \,. \end{aligned} \tag{17}$$

By identifying the real part of Eq. (17) with Eq. (15) one can determine both the spectral density and the imaginary part of the quantum correlation function, i.e.,

$$J_n(\omega) = 2\tanh(\beta\omega/2) \int_0^{\infty} dt\, C_n(t) \cos\omega t, \tag{18}$$

and

$$\mathscr{C}_n''(t) = \int_0^{\infty} \frac{d\omega}{\pi} J_n(\omega) \sin\omega t. \tag{19}$$

Thus, the lineshape function within the second cumulant approximation is

$$A_n(\omega) \equiv \overline{A}_n(\omega - \omega_n) = \int_0^{\infty} dt\, e^{-\phi_n(t)} \cos[(\omega - \omega_n)t + \varphi_n(t)], \tag{20}$$

where the broadening and frequency shift functions are given by

$$\phi_n(t) = \int_0^t d\tau\, (t-\tau) C_n(\tau) \,, \tag{21}$$

and

$$\varphi_n(t) = \int_0^{\infty} \frac{d\omega}{\pi} J_n(\omega) \frac{\omega t - \sin\omega t}{\omega^2} \,. \tag{22}$$

Formally Eq. (20) and (8) for the lineshape function and the OD spectrum remain valid in the case of N excitonically coupled pigment molecules as well provided that the site index n is replaced with the excitonic index J. In principle the energies $\mathscr{E}_{J,\lambda_J}$ and TDMs $\mathbf{d}_J$ of the excitonic states $|J;\lambda_J\rangle$, $J = 1,\ldots,N$, ought to

be determined from QC calculations by considering all N pigments as a single quantum system. Since such computational approach is still prohibitively expensive a practical alternative is to use an *effective Hamiltonian* for determining the time series $\Delta E_J(t) = \mathscr{E}_J(t) - \mathscr{E}_0(t)$ and $\mathbf{d}_J(t)$ from $\Delta E_n(t)$ and $\mathbf{d}_n(t)$ of the individual pigments. Assuming that the latter interact via a point dipole-dipole interaction

$$V_{nm} = \frac{1}{4\pi\varepsilon_0\varepsilon_r}\left[\frac{\mathbf{d}_n\mathbf{d}_m}{r_{nm}^3} - 3\frac{(\mathbf{d}_n\cdot\mathbf{r}_{nm})\,(\mathbf{d}_m\cdot\mathbf{r}_{nm})}{r_{nm}^5}\right], \tag{23}$$

where ε_r is the relative dielectric permitivity of the medium, $\mathbf{r}_n$ is the position vector of pigment n, and $\mathbf{r}_{nm} = \mathbf{r}_m - \mathbf{r}_n$, the eigenvalue equation one needs to solve at every MD timestep is

$$\sum_m [(\Delta E_n\delta_{nm} + V_{nm}) - \Delta E_J\delta_{nm}]c_m^{(J)} = 0\,. \tag{24}$$

In term of the coefficients $c_n^{(J)} = \langle J|n\rangle$ the excitonic TDMs are

$$\mathbf{d}_J = \sum_n \langle J|n\rangle\,\mathbf{d}_n\,. \tag{25}$$

Next, by rewriting the Hamiltonian (2) in diagonal form (i.e., in terms of noninteracting excitons) $H = \sum_J H_J = \sum_{J,\lambda_J} |J;\lambda_J\rangle\mathscr{E}_{J,\lambda_J}\langle J;\lambda_J|$, it follows

$$\left\langle \hat{\mu}_{m,j}^{\dagger}(0)\hat{\mu}_{n,i}(t)\right\rangle = \sum_J \langle J|n\rangle d_{n,i}d_{m,j}\langle m|J\rangle\left\langle e^{iH_0t}e^{-iH_Jt}\right\rangle, \tag{26}$$

and

$$\sum_{n,m}\left\langle \hat{\mu}_{m,j}^{\dagger}(0)\hat{\mu}_{n,i}(t)\right\rangle = \sum_J d_{J,i}d_{J,j}\left\langle e^{iH_0t}e^{-iH_Jt}\right\rangle. \tag{27}$$

Inserting Eq. (27) into Eq. (5) one obtains the desired OD spectrum of the excitonic system

$$I(\omega) \propto \omega\sum_J d_J^2 A_J(\omega)\,, \tag{28}$$

where

$$A_J(\omega) = \mathrm{Re}\int_0^{\infty} dt e^{i\omega t}\left\langle e^{iH_0t}e^{-iH_Jt}\right\rangle. \tag{29}$$

B. Polaron model

An alternative approach for calculating the OD spectrum of a PPC at finite temperature is based on the so-called *polaron model*, according to which the excitonically coupled pigment molecules (excitons) interact with the vibronic modes (phonons) of the system [7, 25]. The corresponding model Hamiltonian

[37], in the second quantized, site representation reads

$$H = H_{ex} + H_{ph} + H_{int} \,, \tag{30}$$

$$H_{ex} = \sum_n \varepsilon_n B_n^\dagger B_n + \sum_{n \neq m} V_{nm} B_n^\dagger B_m = \sum_J E_J B_J^\dagger B_J \,, \tag{31}$$

$$H_{ph} = \sum_{n,\alpha} \omega_\alpha b_{n\alpha}^\dagger b_{n\alpha} \,, \tag{32}$$

$$H_{int} = \sum_{n\alpha} g_\alpha \omega_\alpha B_n^\dagger B_n (b_{n\alpha}^\dagger + b_{n\alpha}) \,. \tag{33}$$

In the exciton Hamiltonian H_{ex} the operator $B_n^\dagger$ (B_n) creates (destroys) an electronic excitation ε_n on the n^{th} pigment (modeled as a two level system), while V_{nm} describes the excitonic coupling between the pigments n and m. The eigenstates of H_{ex} are *excitons* (delocalized electronic excitations) characterized by the creation (annihilation) operator $B_J^\dagger$ (B_J) and energy E_J. The index $J = 1, \ldots, N$ labels the excitonic states upon increasing energy. Similarly, the operator $b_{n\alpha}^\dagger$ ($b_{n\alpha}$) in the phonon Hamiltonian H_{ph} creates (annihilates) a vibronic mode ω_α at site n. Finally, H_{int} describes the interaction between excitons and phonons. For simplicity one assumes that both the phonon spectrum ω_α and the exciton-phonon coupling constant g_α are site independent. The stationary states corresponding to (31) are excitons "dressed" with a phonon cloud and are referred to as *polarons*. The parameters in the polaron model, i.e., ε_n, V_{nm}, g_α and ω_α, ought to be determined either empirically or from combined MD/QC simulations.

To illustrate the calculation of the OD spectrum within the framework of the polaron model, for simplicity, one assumes that all pigments are identical (i.e., ε_n and the TDMs d_n are the same for each pigment). Formally, by replacing the site index n with J, the OD spectrum is given by Eqs. (7),(8) and (13), with $\Delta H_J = H_{ex} + H_{int}$. Using Eq. (31) one finds

$$\langle \Delta H_J \rangle = E_J \equiv \omega_J \,, \tag{34}$$

and

$$\mathscr{C}_J(t) = \langle \delta H_J(t) \delta H_J(0) \rangle = \langle H_{int}(t) H_{int}(0) \rangle = \sum_{n,\alpha} g_\alpha^2 \omega_\alpha^2 \langle \rho_n(t) \rho_n(0) \rangle \langle A_{n\alpha}(t) A_{n\alpha}(0) \rangle \,, \tag{35}$$

where, by definition, the electronic excitation number operator $\rho_n(t) = e^{iH_{ex}t} B_n^\dagger B_n e^{-iH_{ex}t}$, and the phonon field operator $A_{n\alpha}(t) = b_{n\alpha}^\dagger e^{i\omega_\alpha t} + b_{n\alpha} e^{-\omega_\alpha t}$. In terms of the Bose-Einstein distribution function, $N(\omega) = 1/(e^{\beta\omega} - 1)$, the (site independent) phonon field correlation function in Eq. (35) can be expressed as [4, 7, 31]

$$\begin{aligned} D_{\omega_\alpha}(t) \equiv \langle A_{n\alpha}(t) A_{n\alpha}(0) \rangle &= [N(\omega_\alpha) + 1] e^{-i\omega_\alpha t} + N(\omega_\alpha) e^{i\omega_\alpha t} \\ &= \coth(\beta\omega_\alpha/2) \cos(\omega_\alpha t) - i \sin(\omega_\alpha t) \,. \end{aligned} \tag{36}$$

The excitonic factor in the correlation function (35) can also be readily calculated with the result

$$F_J(t) = \sum_n \langle \rho_n(t)\rho_n(0)\rangle = \sum_{J'} e^{i(E_J - E_{J'})t} \sum_n |\langle n|J\rangle|^2 |\langle n|J'\rangle|^2 \,. \tag{37}$$

In general, $|F_J(t)| < 1$ and this factor is responsible for the so-called *exchange narrowing* of the lineshape function. In the absence of excitonic coupling between pigments, i.e., $V_{nm} \approx 0$, the index J in (37) identifies with a particular site index $m = 1,\ldots,N$, resulting in $F_{J=m}(t) = 1$, i.e., as expected, there is no exchange narrowing. Next, by introducing the *phonon spectral density*

$$J(\omega) = \pi \sum_\alpha g_\alpha^2 \omega_\alpha^2 \delta(\omega - \omega_\alpha) = \pi\omega^2 \sum_\alpha g_\alpha^2 \delta(\omega - \omega_\alpha) \,, \tag{38}$$

the sought quantum correlation function (35) assumes the general form

$$\mathscr{C}_J(t) = F_J(t)\mathscr{C}_n(t) \,, \tag{39}$$

where

$$\mathscr{C}_n(t) = \int_0^\infty \frac{d\omega}{\pi} J(\omega) \left[\coth(\beta\omega/2)\cos(\omega t) - i\sin(\omega t)\right] \,. \tag{40}$$

As mentioned before, in the absence of excitonic coupling $F_J(t) = 1$, and Eqs. (39)-(40) formally coincides with Eq. (17), thus suggesting that in this case the polaron model approach and the correlation function method described in Sec. II A for calculating OD spectra are equivalent. However, in principle, the latter approach is more general than the former because it treats the environment beyond the harmonic heat bath approximation, albeit within the cumulant approximation. The determination of $J(\omega)$ from Eq. (38) requires the seemingly unattainable knowledge of the energies ω_α of *all* phonons, together with their corresponding coupling constants g_α. This problem is similar to the spin-boson model description of the coupling between protein motion and electron transfer processes [38] that can be solved by evaluating the spectral function from the energy gap fluctuations $\delta E_n(t)$ as described in the previous sections. On the other hand, Eq. (38) provides a simple physical interpretation of the spectral function. Indeed, if one regards the environment in a PPC as an equivalent harmonic-phonon heat bath then one can interpret the magnitude of the spectral functions as a measure of the coupling strength to phonons of that particular frequency. In general, the complex structure of the spectral function (determined from the combined MD/QC calculations according to Eq. (18); see also Fig. 5b) indicates that all inter and intra molecular vibronic modes within a wide range of frequencies will contribute to the lineshape function. Hence, attempts to use simplified model spectral functions appear to be unrealistic even if these may lead to absorption spectra that match the experimental results.

C. Circular dichroism

By definition, the CD spectrum $I_{CD}(\omega)$ is the difference between $I_L(\omega)$ and $I_R(\omega)$, the OD spectra for left and right circularly polarized light, respectively. Unlike in the case of the OD spectrum, the calculation of $I_{CD}(\omega)$ even within the leading order approximation requires taking into account the spatial variation of the light field across the PPC as well as the excitonic coupling between the pigment molecules regardless how small this may be [16]. The sensitivity of the CD spectrum to geometrical and local details of the PPC makes it a quantity difficult to predict by theoretical modeling. The CD spectrum is given by[5]

$$\begin{aligned} I_{CD}(\omega) = \frac{1}{4}[I_L(\omega) - I_R(\omega)] \propto \omega \,\mathrm{Re} \int_0^\infty dt\, e^{i\omega t} \\ \times \sum_{n,m} \frac{\pi}{\lambda} \varepsilon_{ijk} (\mathbf{r}_n)_k \left\langle \hat{\mu}^\dagger_{m,i}(0) \hat{\mu}_{n,i}(t) \right\rangle \end{aligned} \tag{41}$$

where λ is the wavelength of the incident light and ε_{ijk} is the unit antisymmetric tensor of rank 3. Inserting Eq. (26) into (41) and making use of Eq. (29), one obtains

$$I_{CD}(\omega) \propto \omega \sum_J R_J A_J(\omega) \,, \tag{42}$$

where

$$R_J = \frac{\pi}{\lambda} \sum_{n,m} \langle J|n\rangle [\mathbf{r}_n \cdot (\mathbf{d}_n \times \mathbf{d}_m)] \langle m|J\rangle \tag{43}$$

is the so-called *rotational strength* of the excitonic state J. It should be noted that in the absence of the excitonic coupling all $R_J = 0$ (because for a given J only one coefficient $\langle J|n\rangle$ is nonzero) and the CD spectrum vanishes. The rotational strength plays the same role for the CD spectrum as the TDM strength for the OD spectrum. Specifically, R_J gives the coupling between the TDM of the excitonic state J and the orbital magnetic moment of the other excitons. The coupling to the local magnetic moment is assumed to be small (Cotton effect) and usually is discarded [16, 39].

III. ELECTRON TRANSFER AT FINITE TEMPERATURE

Another important class of quantum processes in PPCs involves electrons switching between two states. Two examples are electron transfer reactions in PPCs when an electron moves from an orbital on the donor moiety D to an orbital on the acceptor moiety A and bond formation or bond breaking in an enzyme when electrons shift from a non-bonding state to a bonding state or vice versa. Here only the electron trasfer processes will be considered. An ideal PPC system for studying the electron transfer process is the photosynthetic reaction center (PRC) in photosynthetic bacteria. For quite some time high resolution crystal

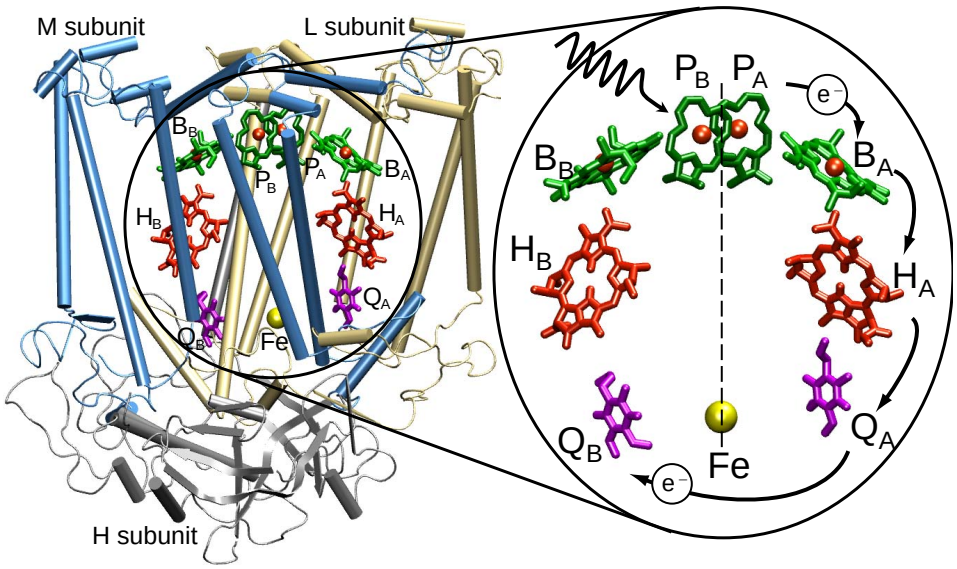

FIG. 2: **Left:** Structure of the PRC of *Rb. sphaeroides* (entry code 1PCR in Protein Data Bank). For clarity only the backbone of the protein subunits L, M and H are shown. The protein helices are represented by cylinders. The cofactors are labeled, and for clarity their phytyl tails are not shown. **Right:** Spatial distribution of the cofactors in the PRC. The path of the electrons through the PRC is indicated by the arrows. Graphics rendered with the program VMD [29].

structures are available for PRCs from several species of photosynthetic bacteria, such as *Rhodobacter (Rb.) sphaeroides* [40] shown in Fig. 2. In general, PRCs are formed by three protein subunits, denoted L, M and H. The H subunit is located on the cytoplasmic side of the cell membrane and is anchored to it by a single transmembrane helix. The homologous L and M subunits have five transmembrane helices and display a quasi-twofold rotational symmetry. Several photoactive pigment molecules (termed as co-factors or prosthetic groups) are bound by the L and M subunits in a symmetric fashion and being labeled A and B, respectively. These cofactors, which play a key role in the electron transfer processes within the PRC, consist of (Fig. 2): two BChls that form a strongly interacting dimer called the *special pair* (P_A, P_B); two monomeric BChls (B_A, B_B) located near the special pair; two bacteriopheophytins (H_A, H_B); a pair of *ubiquinone* molecules (Q_A, Q_B); and one non-heme iron atom (Fe) [40]. The main steps involved in photosynthetic charge separation in the PRC are as follows: (i) the special pair (the primary electron donor) is excited through the absorption of an incident photon, and then relaxes by transferring an electron through B_A to H_A in ~ 3 ps; (ii) the electron is transferred from H_A^- to Q_A in ~ 200 ps; (iii) Q_A^- transfers an electron to Q_B in ~ 200 μs by converting the latter into a semiquinone radical; (iv) during this time the positively charged special pair is neutralized by extracting an electron from a monoheme c-type cytochrome (cyt c_2) on the periplasmic side of the membrane (this soluble cytochrome shuttles the electron between the cyt bc_1

complex and the PRC); (v) when another incoming photon is absorbed by the special pair, a second electron flows to Q_B^- via the same pathway; (vi) this time Q_B^{2-} is converted into *quinol* (hydroquinone Q_BH_2) by the simultaneous uptake of two protons from the cytoplasmic side of the complex; (vii) the quinol diffuses out of the PRC and into the cell membrane that is rich in mobile quinones; (viii) the cycle of electron transfer is completed by the oxidation of the quinol by the cyt bc_1 complex which results in the transfer of protons across the membrane and the re-reduction of cyt c_2. The transmembrane proton gradient drives the synthesis of ATP, the universal fuel molecule, by ATP synthase.

The electron transfer process can also be formally regarded as a chemical reaction $AD \rightarrow A^+D^-$, where AD and A^+D^- are the reactant and product states, respectively. The energy expectation values of the two states, $E_1(t)$ and $E_2(t)$, vary in time due to motions along a reaction coordinate, but also due to thermal fluctuations of the remaining degrees of freedom of the PPC. Often the interaction energies which couple the two electronic states involved in the reaction are small compared to the temporal variations of $E_1(t)$ and $E_2(t)$. In this rather typical case the actual reaction process is confined to moments when the two electronic states become energetically degenerate [$E_1(t) = E_2(t)$]. Such *curve crossing* processes in PPCs are strongly dependent on the thermal motion of the entire system including the protein matrix, the solvent and the lipid membrane in case of membrane bound PPCs. In a quantum mechanical description, one defines the Hamiltonians H_1 and H_2 that describe the collective motion of the system in the reactant (initial) and product (final) electronic states of the PPC. The weak coupling between the two can be described by a tunneling matrix element V.

Just like in the case of optical absorption spectra, the effect of dynamic disorder on the electron transfer processes in PPCs can also be determined by employing the combined MD/QC method described in the previous section. Once the A and D moieties have been identified the time series of the electronic ground state energies $E_{1,2}(t_i)$, $i = 0, 1, \ldots$, of the two redox states can be determined by QC calculation for each snapshot t_i along the MD trajectory.

A. Cumulant approximation of the electron transfer rate

Assuming that the tunneling matrix element V does not change significantly due to the thermal motion of the protein matrix (Condon approximation), within the lowest order of perturbation theory in V the electron transfer rate k_{ET} in a PPC can be expressed as [31]

$$k_{ET} = |V|^2 \int_{-\infty}^{\infty} dt \, \left\langle e^{iH_1 t} e^{-iH_2 t} \right\rangle \tag{44}$$

Similarly to Eq. (13), by employing the cumulant approximation

$$k_{ET} \approx |V|^2 \int_{-\infty}^{\infty} dt \exp\left[-i\langle\Delta H\rangle t - \int_0^t d\tau (t-\tau)\mathscr{C}(\tau)\right] \tag{45}$$

where $\Delta H \equiv H_2 - H_1$, $\Delta H(t) = e^{iH_1 t}\Delta H e^{-iH_1 t}$, $\mathscr{C}(t) = \langle \delta H(t)\delta H(0)\rangle$, and $\delta H(t) = \Delta H(t) - \langle \Delta H\rangle$. By following the same methodology as in the derivation of the OD spectrum of a PPC [cf. Eqs. (14),(15) and (20)] the electron transfer rate can be brought to the form

$$k_{ET} = 2|V|^2 \int_0^{\infty} dt\, e^{-\phi(t)} \cos[\varepsilon t - \varphi(t)]\,, \tag{46}$$

where $\varepsilon = \langle \Delta H\rangle \approx \langle \Delta E(t)\rangle$ is the mean energy gap,

$$\phi(t) = \int_0^t dt'\,(t-t')C(t)\,, \tag{47}$$

with $C(t) = \mathrm{Re}\mathscr{C}(t) \approx \langle \delta E(t)\delta E(0)\rangle$, and

$$\begin{aligned} \varphi(t) &= -\mathrm{Im}\int_0^t dt'\,(t-t')\mathscr{C}(t') \\ &= \int_0^{\infty} \frac{d\omega}{\pi} J(\omega)\frac{\omega t - \sin\omega t}{\omega^2}\,, \end{aligned} \tag{48}$$

where the spectral function has the usual form

$$J(\omega) = 2\tanh(\beta\omega/2)\int_0^{\infty} dt\, C(t)\cos\omega t\,. \tag{49}$$

Thus, the calculation of k_{ET} and $J(\omega)$ requires in fact only the knowledge of the energy gap time series $\Delta E(t)$ and not those of the individual energies $E_{1,2}(t)$. This simple observation is rather important because most QC methods do not permit the accurate determination of individual energy levels but they can provide energy differences with fairly high precision. A fairly good estimate of the electron transfer rate in PPCs can also be obtained if the energy gap time series $\Delta E(t)$ are determined purely classically instead of combined MD/QC calculations. Knowing the atomic partial charges corresponding to AD and to A^-D^+ one can evaluate $E_1[\mathbf{R}(t)]$ and $E_2[\mathbf{R}(t)]$ along the $\mathbf{R}(t)$ MD trajectory as the Coulomb energies of the acceptor and donor moieties with the protein matrix, to which one adds the redox energies of the states AD and A^-D^+.

In the high temperature limit, one can easily show that the expression of the electron transfer rate derived in this section by applying the cumulant approximation yields in leading approximation the result corresponding to the classical Marcus theory. To show this, one assumes that the correlation function of the energy gap fluctuations has a simple exponential form $C_M(t) = \Delta^2 exp(-t/\tau)$, where $\Delta^2 = \left\langle \delta E^2\right\rangle = \left\langle \Delta E^2\right\rangle - \langle \Delta E\rangle^2$ is the variance of the energy gap fluctuations and τ is the corresponding relaxation time. Thus, the integrals in (47) and (49) can be performed exactly with the results

$$\phi_M(t) = \Delta^2\tau\left[t - \tau\left(1 - e^{-t/\tau}\right)\right] \approx \frac{\Delta^2}{2}t \qquad \text{for} \quad t \ll \tau\,, \tag{50}$$

and

$$J_M(\omega) = 2\tanh(\beta\omega/2)\frac{\beta\Delta^2}{1+(\omega\tau)^2} \approx \frac{\beta\Delta^2\,\omega\tau}{1+(\omega\tau)^2}\ , \tag{51}$$

where the high temperature limit $\beta\omega \ll 1$ has been assumed. Note that the maximum of the spectral function $J_M(\omega)$ corresponds to the energy gap

$$\varepsilon_M = \frac{\beta\Delta^2}{2}\ . \tag{52}$$

Within the same range of approximations the phase factor (48) becomes

$$\varphi_M(t) \approx t\int_0^\infty \frac{d\omega}{\pi}\,\frac{J_M(\omega)}{\omega} = \varepsilon_M t\ . \tag{53}$$

Inserting Eqs (53),(50) into (46) and performing the Gaussian integral, one obtains the well known Marcus formula [31, 41, 42]

$$k_M = 2\sqrt{2\pi}\frac{|V|^2}{\Delta}\exp\left[-\frac{(\varepsilon-\varepsilon_M)^2}{2\Delta^2}\right]\ . \tag{54}$$

Since in general the spectral function (49) has a complex structure [7, 8] the simple exponential approximation of the correlation function $C(t)$ may not be justified so that differences between the electron transfer rates calculated with the simple Marcus formula (54) and with the cumulant approximation (46) may be expected even at high temperatures.

B. Spin-boson model of coupling to a heat bath

Electron transfer between donor and acceptor moieties in a PPC can conveniently be described in terms of the *spin–boson model*. Similarly to the polaron model in the case of optical absorption in PPCs, in the spin–boson model the electronic degrees of freedom are treated as a two state system (one for the reactants and one for the products) and the nuclear degrees of freedom of the protein matrix are approximated by a harmonic heat bath. The name of spin–boson model stems from the fact that the two state electron transfer system is equivalent to a spin–$\frac{1}{2}$ system while the atomic motion is described by a set of independent bosons. Fore example, this model has been successfully applied to investigate the primary electron separation process in the photosynthetic reaction center of *Rhodopseudomonas viridis* by focusing on how the thermal oscillations of the protein atoms couple to the various transfer steps of an electron moving along the prosthetic groups [38]. The key new aspects of the spin–boson model description of electron transfer in PPCs is two-fold: first, all model parameters are determined from molecular dynamics simulations, thus requiring only the knowledge of the atomic resolution crystal structure of the PPC; second, the spin–boson

model accounts for all vibrational modes of the PPC by means of the phonon spectral function that, similarly to the polaron model, can be determined from the time autocorrelation function of the energy gap corresponding to the product and reactant states. The spin–boson model may not only yield qualitatively different predictions than models involving a small number of vibrational modes coupled to the electron transfer, but it certainly makes the role of the medium surrounding an electron transfer reaction appear in a new light: essentially all motions of the environment are coupled significantly to the reaction. The reason is surprisingly simple and applies clearly to the case of a PPC: the coupling between electron transfer and medium is due to the Coulomb interaction. This interaction, however, is long range and encompasses a very large volume. The coupling results then from small additive contributions of many motions rather than from a few dominant modes.

A detailed review of the theory of the spin–boson model can be found in [43]. In the case of a PPC the electron transfer reaction is described in terms of the two–state Hamiltonian, written both in first and second quantized forms

$$\hat{H}_{el} \;=\; V\,\sigma_x \;-\; \frac{1}{2}\,\varepsilon\,\sigma_z = \sum_{n=1}^{2} \varepsilon_n\, B_n^{\dagger} B_n + \sum_{n\neq m=1}^{2} V\, B_n^{\dagger} B_m \;, \tag{55}$$

where σ_x, σ_z are the usual 2×2 Pauli matrices, $\varepsilon = \varepsilon_2 - \varepsilon_1$ is the difference of product state ε_2 and reactant state ε_1 energies (energy gap), V accounts for the coupling between reactant and product states (the coupling originating from tunneling of the electron between electron donor and electron acceptor moieties), and $B_{1,2}$ ($B_{1,2}^{\dagger}$) are the annihilation (creation) fermionic operators of the two redox states. The medium thermal motion is described through an ensemble of independent harmonic oscillators (phonons) with the Hamiltonian

$$H_{ph} = \sum_{\alpha} \sum_{n=1}^{2} \omega_\alpha\, b_{n\alpha}^{\dagger}\, b_{n\alpha} \;. \tag{56}$$

Here $b_{n,\alpha}$ ($b_{n,\alpha}^{\dagger}$) creates (destroys) a phonon (vibronic) mode with frequency ω_α in the n-th redox state. The coupling between the vibrational degrees of freedom and the two–state system is linear

$$H_{int} = \sum_{\alpha} \sum_{n=1}^{2} g_\alpha \omega_\alpha\, B_n^{\dagger} B_n\, (b_{n\alpha}^{\dagger} + b_{n\alpha}) \;. \tag{57}$$

where g_α describes the strength of the coupling of the electron transfer to the α-th mode. The spin–boson Hamiltonian is the sum of all three contributions, i.e.,

$$H_{sb} = H_{el} + H_{ph} + H_{int} \;. \tag{58}$$

One may worry at this point that the many parameters which appear in the spin–boson model are impossible to specify uniquely and therefore, the model is either arbitrary or of limited use. However, just like in

the case of the polaron model [7, 8] described above, the value of the spin–boson model [43] lies in the fact that the electron transfer rate can be determined uniquely in terms of the spectral function

$$J_{sb}(\omega) = \pi\omega^2 \sum_{\alpha} g_{\alpha}^2 \delta(\omega - \omega_{\alpha}) \; , \tag{59}$$

the energy gap ε and the coupling V. Note that Eq. (59) is formally identical with (38), and it can be determined from the real time autocorrelation function $C(t) \approx \mathrm{Re}[\mathscr{C}(t)]$ of the energy gap fluctuations, $\delta\varepsilon(t) = \varepsilon(t) - \langle\varepsilon\rangle$, by means of Eq. (18).

The energy gap time series $\varepsilon(t)$ and the coupling V can be computed either from classical MD simulations or from combined MD/QC calculations. Once $C(t)$ and $J_{sb}(\omega)$ have been determined, the electron transfer rate k_{sb} can be readily calculated by means of Eqs. (46)-(48).

IV. SIMULATION OF OPTICAL EXCITATIONS

According to the results presented in Sec. II in order to calculate the OD and CD spectra of the B800 and B850 BChls in a single LH2 ring from *Rs. molischianum* first one needs to determine the time series of the Q_y energy gap $\Delta E_n(\ell\Delta t)$ and TDM $\mathbf{d}_n(\ell\Delta t)$, $\ell = 0, 1, \ldots, N_t$, for all individual BChls. This requires two steps: (1) use all atom MD simulations to follow the dynamics of the nuclear degrees of freedom by recording snapshots of the atomic coordinates at times $t_\ell = \ell\Delta t$, and (2) use QC calculations to compute ΔE_n and $\mathbf{d}_n$ for each snapshot [7, 8].

A. Molecular dynamics simulations

The first MD simulation of the LH2 antenna complex from *Rs. molischianum* embedded in a fully solvated lipid bilayer mimicking its native environment was reported in Ref. 7. A perfect 8-fold LH2 ring was constructed starting from the crystal structure (pdb code 1LGH) of *Rs. molischianum* [10] (see Fig. 1). After adding the missing hydrogens, the protein system was embedded in a fully solvated POPC lipid bilayer of hexagonal shape. A total of 16 Cl^- counterions were properly added to ensure electroneutrality of the entire system of 87,055 atoms. In order to reduce the finite-size effects, the hexagonal unit cell (with side length ~ 60Å, lipid bilayer thickness ~ 42Å and two water layers of combined thickness ~ 35Å) was replicated in space by using periodic boundary conditions. The CHARMM27 force field parameters for proteins [44, 45] and lipids [46] were used. Water molecules were modeled as TIP3P [47]. The ground state ESP partial charges for geometry optimized BChls without phytyl tail were determined with the program JAGUAR [48]. The force field parameters for BChls were taken from [49, 50] and for lycopenes were determined using the program QUANTA [51]. After energy minimization, the system was subjected to a 2 ns

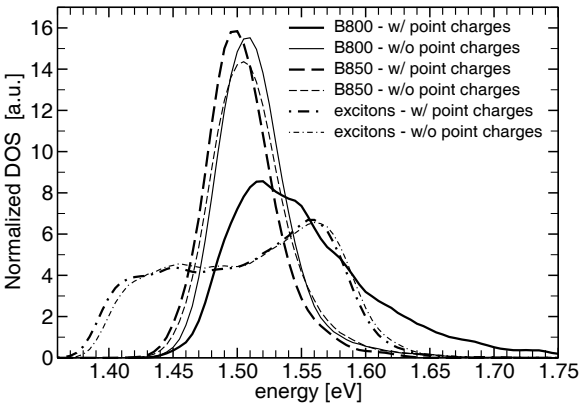

FIG. 3: Normalized DOS, $\mathscr{N}(\omega)$, for individual B800 BChls (solid-line), B850 BChls (dashed-line), and B850 excitons (dashed-dotted-line) in LH2 from *Rs. Molischianum* computed as binned histograms of the corresponding Q_y excitation energy time series obtained from combined MD/QC simulations. Whether the charge fluctuations of the BChls' environment are included (thick-lines) or not (thin-lines) make an important difference in $\mathscr{N}(\omega)$ only for B800.

long equilibration in the NpT ensemble [52] at normal temperature ($T = 300$ K) and pressure ($p = 1$ atm), using periodic boundary conditions and treating the full long-range electrostatic interactions by the PME method [53]. All MD simulations were preformed with the program NAMD 2 [54], with a performance of ~ 8.5 days/ns on 24 CPUs of an AMD 1800+ Beowulf cluster. During equilibration an integration time step of 2 fs was employed by using the SHAKE constraint on all hydrogen atoms [55]. After the 2 ns equilibration a 1 ps production run with 1 fs integration step was carried out with atomic coordinates saved every other timestep, resulting in $N_t = 500$ MD snapshots with $\Delta t = 2$ fs time separation. These configuration snapshots were used as input for the QC calculations.

B. Quantum chemistry calculations

The time series of the Q_y transition energies ΔE_n and dipole moments $\mathbf{d}_n$ of individual BChls can be determined only approximately from the configuration snapshots obtained from MD simulations. The level of approximation used is determined by: (i) the actual definition of the optically active *quantum system*, i.e., the part of the system that is responsible for light absorption and needs to be treated quantum mechanically; (ii) the actual choice of the QC method used in the calculations; and (iii) the particular way in which the effect of the (classical) environment on the quantum system is taken into account in the QC calculations. Because the optical properties of BChls are determined by the cyclic conjugated π-electron system of the macrocycle the quantum system was restricted to a truncated structure of the BChl restricted to the porphyrin plane [8, 9, 56]. Although in general the different truncation schemes yield excitation energy time series

with shifted mean values, the corresponding energy fluctuations, which play the main role in calculating the optical absorption properties of PPC at room temperature in their native environment, are less sensitive to the actual size of the truncated pigment. On the other hand, however, the required computational effort can be reduced dramatically through such truncation of the quantum system.

The preferred method for calculating the Q_y excitations of the truncated BChls is Zerner's semiempirical intermediate neglect of differential overlap method parametrized for spectroscopy (ZINDO/S) within the single-point configuration interaction singles (CIS) approximation [57, 58]. Because it is much faster and more accurate than most of the computationally affordable *ab initio* QC methods (e.g., the Hartree-Fock (HF) CIS method with the minimal STO-3G* basis set), ZINDO/S CIS has been extensively used in the literature to compute low lying optically allowed excited states of pigment molecules [8, 22, 24, 59, 60]. The ZINDO/S method is integral part of standard QC program packages such as HyperChem [61] and GAUSSIAN 98 [62].

The effect of the environment on the quantum system can be taken into account through the electric field created by the partial point charges of the environment atoms, including those BChl atoms that were removed during the truncation process. Thus, the dynamics of the nuclear degrees of freedom (described by MD simulation) have a two-fold effect on the fluctuations of the Q_y state, namely they lead to: (1) conformational fluctuation of the (truncated) BChls, and (2) a fluctuating electric field created by the thermal motion of the corresponding atomic partial charges. The relative importance of these two effects on the time series $\Delta E_n(t)$ were estimated by performing the QC calculations both in the presence and in the absence of the point charges [8]. For each case, a total of 12,000 (500 snapshots $\times$ 24 BChls) ZINDO/S calculations were performed with a performance of ~ 2.3 min/CPU (~ 0.7 min/CPU) for each calculation with (without) point charges on a workstation with dual 3GHz Xeon EM64T CPU.

C. Energy gap density of states

The 1 ps long time series of the Q_y excitation energies $\Delta E_n(t_\ell)$ and TDMs $\mathbf{d}_n(t_\ell)$, ($t_\ell = \ell\Delta t$; $\ell = 0,\ldots,N_t$; $N_t = 499$; $\Delta t = 2$ fs) computed with the described combined MD/QC method for both B850 ($n = 1,\ldots,16$) and B800 ($n = 17,\ldots,24$) BChls in a LH2 ring from *Rs. molischianum* are sufficiently long for calculating the DOS of the Q_y excitation energies and the corresponding OD and CD spectra [8].

Figure 3 shows the Q_y energy gap DOS, $\mathscr{N}(\omega)$ [Eq. (10)], of the individual B800 (solid-lines) and B850 (dashed-lines) BChls calculated as normalized binned histograms of the time series $\Delta E_{B800} \equiv \Delta E_n(t_\ell)$ with $n = 17,\ldots,24$, and $\Delta E_{B850} \equiv \Delta E_n(t_\ell)$ with $n = 1,\ldots,16$, respectively. In the absence of the point charge distribution of the environment $\mathscr{N}(\omega)$ for B800 and B850 (thin-lines) are almost identical, having peak

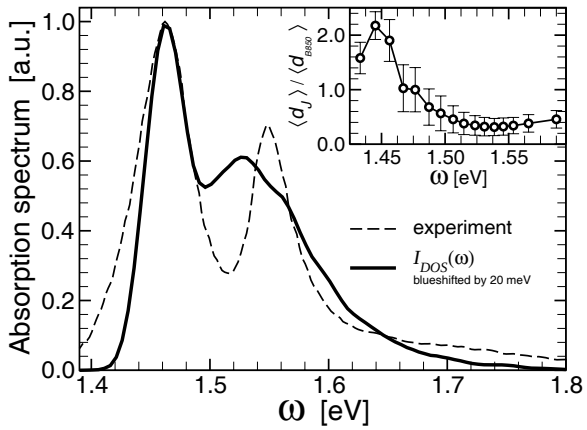

FIG. 4: Absorption spectrum $I_{DOS}(\omega)$ of LH2 for *Rs. molischianum* calculated as a combined DOS of B800 BChls and B850 excitons weighted by the corresponding dipole strengths (solid line). $I_{DOS}(\omega)$ was blueshifted by 20 meV in order to overlay its B850 peak with the corresponding one in the experimental OD spectrum [30] (dashed line). Inset: Average transition dipole moments $\langle d_J \rangle$ corresponding to the $J = 1, \ldots, 16$ B850 excitonic states. Both $\langle d_J \rangle$ and the corresponding error bars are expressed relative to the mean dipole moment of individual B850s.

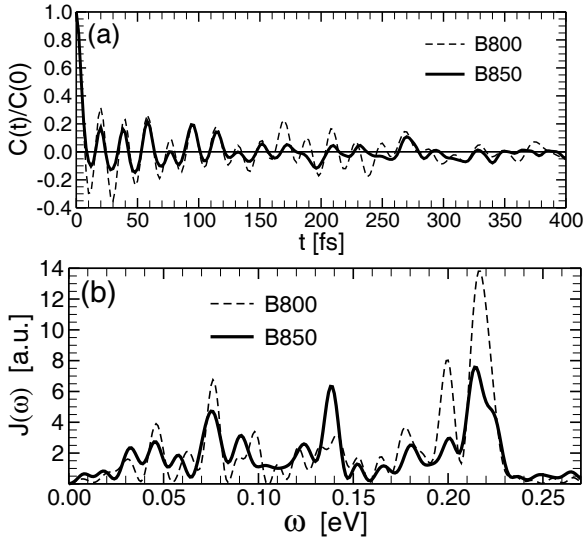

FIG. 5: (a) Normalized autocorrelation function $C(t)/C(0)$ of the energy gap fluctuations $\delta E(t) = E(t) - \langle E \rangle$ for individual B800 (dashed line) and B850 (solid line) BChls, calculated using Eq. . The mean square energy gap fluctuations are $C_{B800}(0) = 3.16 \times 10^{-3}$ eV^2 and $C_{B850}(0) = 8.68 \times 10^{-4}$ eV^2. (b) Spectral density function $J(w)$ for B800 (dashed-line) and B850 (solid-line) obtained according to Eq. (18).

position at 1.51 eV (817 nm) and 1.515 eV (818 nm), and full width at half maximum (FWHM) 51 meV and 59 meV, respectively. It should be noted that essentially the same mean energy gap of 1.5 eV was obtained in similar MD/QC calculations by Mercel et al. [9] for BChl solvated in methanol also at room temperature. These results indicate that the thermal motion of the nuclei in individual BChls lead to Q_y

energy gap fluctuations that are insensitive to the actual nature of the *nonpolar* environment. Since in LH2 from *Rs. molischianum* the B800s (B850s) are surrounded by polar (nonpolar) residues, it is not surprising that once the point charges of the environment are taken into account in the QC calculations $\mathscr{N}(\omega)$ changes dramatically only in the case of B800. Indeed, as shown in Fig. 3, in the presence of the point charges (thick-lines) the peak of $\mathscr{N}_{B850}(\omega)$ is only slightly red shifted to 1.502 eV (825 nm) and essentially without any change in shape with FWHM$\approx$ 53 meV. By contrast, as a result of the point charges the B800 DOS is not only blue shifted but it becomes asymmetric and almost twice as broad with FWHM$\approx$ 100 meV. Thus, in spite of a small blueshift to 1.528 eV (811 nm) of the peak of $\mathscr{N}_{B800}(\omega)$ the mean value of the energy gap $\langle \Delta E_{B800} \rangle = 1.556$ eV (797 nm) is increased considerably, matching rather well the experimental value of 800 nm.

The excitonic energies time series $\Delta E_J(t_\ell)$, $J = 1, \ldots, 16$, of the B850 BChls were determined by solving for each MD snapshot, within the point-dipole approximation, the eigenvalue equation (24). In calculating the matrix elements (23) $\mathbf{r}_n$ was identified with the position vector of the Mg atom in the n-th BChl. Consistent with the Condon approximation, the magnitude of the computed B850 TDM time series exhibited a standard deviation of less than 4% about the average value $\langle d_{B850} \rangle = 11.77$ D. The latter is by a factor of $k = 1.87$ larger than the experimentally accepted 6.3 D value of the Q_y TDM of BChl [63]. By rescaling the TDMs from the ZINDO/S calculations to match their experimental value, and by setting $\varepsilon_r = 1.86$, one obtains for the mean value of the nearest neighbor dipolar coupling energies between B850s 27 meV$\approx$ 220 cm^{-1} within a protomer and 24 meV$\approx$ 196 cm^{-1} between adjacent heterodimers. As expected, the DOS of the excitonic energies (Fig. 3, dashed-dotted-line), computed as a binned histogram of $\Delta E_J(t_\ell)$, is not sensitive to whether the point charges of the environment are included or not in the B850 site energy calculations.

The mean excitonic TDMs, calculated from Eq. (25) and expressed in terms of $\langle d_{B850} \rangle$, are shown as an inset in Fig. 4. The error bars represent the standard deviation of the time series $d_J(t_\ell)$. As expected, most of the dipole strength is amassed into the lowest three excitonic states [7, 8].

According to Eqs. (8) and (9)-(10) a rough estimate of the OD spectrum of the B800 BChls and B850 excitons is given by the corresponding TDM strength weighted DOS

$$I_{DOS}(\omega) \propto \omega \left[\sum_J d_J^2 \langle \delta(\omega - \Delta E_J) \rangle + \sum_{B800} d_{B800}^2 \langle \delta(\omega - \Delta E_{B800}) \rangle \right] , \tag{60}$$

where the $B800$ index in the last term means summation over all B800 BChls. Figure 4 shows the calculated $I_{DOS}(\omega)$ blueshifted by 20 eV (solid-line) in order to match the B850 peak position with the one in the experimental OD spectrum [22, 30] (dashed-line). While the B850 band and the relative heights of the two peaks in $I_{DOS}(\omega)$ match rather well the experimental data, the position and the broadening of the B800

peak do not. This result clearly shows that in general peak positions in optical spectra may be shifted from the corresponding peak positions in the excitation energy spectrum due to correlation effects between the ground and optically active excited states. The latter may also lead to different line broadening of the corresponding peaks. Therefore, methods for simulating optical spectra in which the position of the peaks are identified with the computed excitation energies (stick spectrum) are not entirely correct and using instead more sophisticated methods that include quantum correlation effects should be preferred.

D. Linear absorption spectrum

According to Eq. (20) and (18) the lineshape functions of the individual B850 and B800 BChls is the (classical) autocorrelation function $C_n(t) = \langle \delta E_n(t) \delta E_n(0) \rangle$ of the energy gap fluctuation $\delta E_n(t) = \Delta E_n(t) - \langle \Delta E_n \rangle$ determined from combined MD/QC calculations. Since the LH2 ring from *Rs. molischianum* has an eight-fold symmetry, for best statistics one calculates a single time correlation function $C_{B800}(t)$ [$C_{B850}(t)$] by averaging over all B800 [B850] BChls according to the formula

$$\begin{gathered} C_\alpha(t_\ell) = \frac{1}{M} \sum_m \left[\frac{1}{N_t - \ell} \sum_{k=1}^{N_t - \ell} \delta E_m(t_\ell + t_k) \delta E_m(t_k) \right] , \\ \text{where } M = 8,\ m = 17, \ldots, 24 \ \text{ for } \ \alpha = B800 \, , \\ \text{and } M = 16,\ m = 1, \ldots, 16 \ \text{ for } \ \alpha = B850 \, . \end{gathered} \tag{61}$$

The normalized correlation functions $C_\alpha(t)/C_\alpha(0)$, $\alpha \in \{B800, B850\}$, are plotted in Fig. 5a. $C_\alpha(0) = \langle \delta E^2 \rangle$ represents the variance of the energy gap fluctuations with $C_{B800}(0) = 3.16 \times 10^{-3}$ eV^2 and $C_{B850}(0) = 8.68 \times 10^{-4}$ eV^2. Both correlation functions have a qualitatively similar behavior with the following features: (i) sharp decay to negative values in the first 9 fs, (ii) a ~ 18.5 fs period oscillatory component with uneven amplitudes, and (iii) vanishingly small magnitude after $t \gtrsim 400$ fs. The spectral densities $J_\alpha(\omega)$ for B800 and B850, determined according to Eq. (18), are shown in Fig. 5b. The prominent peak about $\omega_p = 0.22$ eV is due to the fast initial decay of $C_\alpha(t)$ and it is most likely due to strong coupling of the pigment to an intramolecular C=O vibronic mode [7, 9]. The complex structure of the spectral functions indicate that all inter and intra molecular vibronic modes with frequency below ω_p will contribute to the lineshape function. Hence, attempts to use simplified model spectral functions appear to be unrealistic even if these may lead to absorption spectra that match the experimental results.

The lineshape functions of individual B800 and B850, calculated from Eq. (20), are plotted in Fig. 6a. The origin of the frequency axis corresponds to the mean energy gaps ω_{B800} and ω_{B850}, respectively. The highly polarized surrounding of the B800 BChls in *Rs. molischianum* renders $A_{B800}(\omega)$ twice as broad (FWHM$\approx$ 26 meV) as $A_{B850}(\omega)$ (FWHM$\approx$ 13 meV). Also, the redshift of the peak of the former ($\Delta\omega \approx$

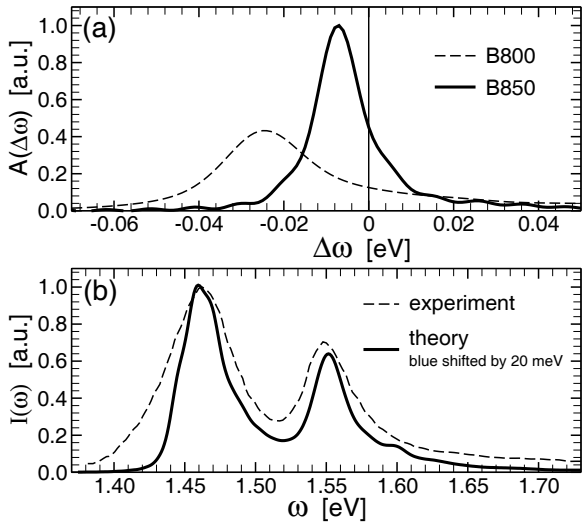

FIG. 6: (a) Lineshape functions $\overline{A}_{B800}(\Delta\omega)$ (dashed line) and $\overline{A}_{B850}(\Delta\omega)$ (solid line). (b) Computed (solid line) and experimental (dashed line) absorption spectra (in arbitrary units) of the BChl aggregate in *Rs. Molischianum* LH2. The computed spectrum has been blue shifted by 20 meV for best match.

25 meV) is more than three times larger than that of the latter ($\Delta\omega \approx 7$ meV).

Although the 1 ps long energy gap time series provide a proper estimate of the B800 and B850 lineshape functions, the same data is insufficient to determine with reasonable accuracy the individual excitonic lineshape functions $A_J(\omega)$. Thus, by neglecting the effect of *exchange narrowing* [16, 39], one can approximate $A_J(\omega) \approx A_{B850}(\omega)$, and the OD spectrum of the LH2 BChls becomes

$$I(\omega) \propto \omega \left[\sum_J d_J^2 \overline{A}_{B850}(\omega - \omega_J) + 8 d_{B800}^2 \overline{A}_{B800}(\omega - \omega_{B800}) \right] , \tag{62}$$

where $\omega_J = \langle \Delta E_J \rangle$. As shown in Fig. 6b, $I(\omega)$ (subject to an overall blueshift of 20 meV) matches remarkably well the experimental OD spectrum, especially if we take into account that it was obtained from the sole knowledge of the high resolution crystal structure of LH2 from *Rs. molischianum* [8]. The reason why both B800 and B850 peaks of $I(\omega)$ are somewhat narrower than the experimental ones is most likely due to the fact that the effect of static disorder is ignored. Indeed, our calculations were based on a single LH2 ring, while the experimental data is averaged over a large number of such rings. While computationally expensive, in principle, the effect of static disorder could be taken into account by repeating the above calculations for different initial configurations of the LH2 ring and then averaging the corresponding OD spectra.

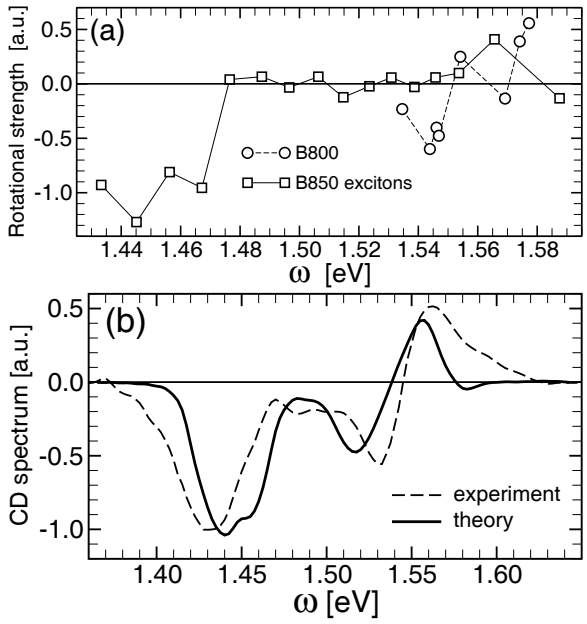

FIG. 7: (a) Mean rotational strength of the excitonically coupled B800 (circle) and B850 (box) BChls as a function of the corresponding excitonic energies. The purpose of the thin lines are to guide the eye. (b) Comparison between the computed (solid line) and experimental CD spectrum of the BChl aggregate in *Rs. Molischianum* LH2.

E. Circular dichroism spectrum

Using the results from Sec. II C, the calculation of the CD spectrum of the LH2 BChls proceeds along the following two steps [8].

First, the rotational strength of both B850 excitons and B800 BChls is determined using Eq. (43). Here, just like in the case of the point-dipole interaction matrix elements (23), $\mathbf{r}_n$ represents the position vector of the Mg atom in the n^{th} BChl. The calculation of the rotational strength of the B800 BChls requires solving the corresponding excitonic Hamiltonian (24) regardless how small the dipole-dipole coupling is between these BChls. The calculation does not yield either noticeable corrections to the B800 excitation energies or admixture of the corresponding Q_y states, however, it leads to sizable mean rotational strengths as shown in Fig. 7a (filled circles). Similarly to the TDM strengths, the largest (negative) mean rotational strengths are carried by the four lowest B850 excitonic states as shown in Fig. 7a (open squares). The second highest excitonic state also has a sizable rotational strength and is responsible for enhancing the positive peak of the B800 contribution to the CD spectrum.

Second, the CD spectrum is calculated from Eq. (42) where the summation index J runs over all B850 and B800 excitonic states and $A_J(\omega) = \overline{A}_\alpha(\omega - \omega_J)$, with $\alpha \in \{B850, B800\}$. The obtained CD spectrum is shown in Fig. 7b (solid-line) and it appears to match fairly well the experimental spectrum (dashed line)

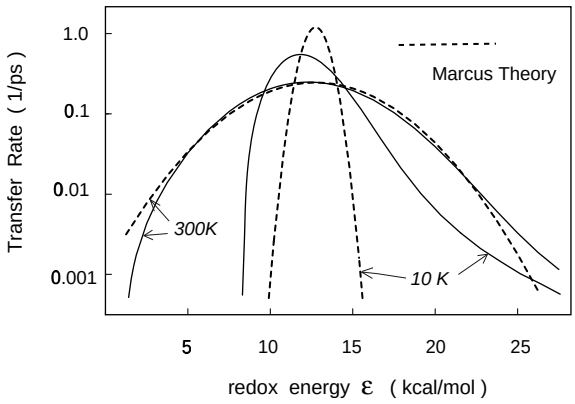

FIG. 8: Comparison of electron transfer rates $k(\varepsilon;T)$ shown as a function of ε evaluated in the framework of the spin-boson model (solid lines) and by Marcus theory (dashed lines) at temperatures 10 K and 300 K. The functions are centered approximately around ε_M.

[22]. It should be emphasized that apart from an overall scaling factor the CD spectrum was calculated from the same MD/QC data as the OD spectrum by following the procedure described above.

V. CALCULATION OF ELECTRON TRANSFER RATES

A detailed study of electron transfer rates k_{ET} in the photosynthetic reaction center of *Rhodopseudomonas viridis* by employing the spin-boson model was reported in Refs. [38, 64]. The model parameters Δ and τ were determined by means of all atom MD simulations. Due to large errors in calculating the mean redox energy gap ε the authors used this as a fitting parameter. The calculated $k_{ET}(\varepsilon;T)$ for temperatures $T = 10$ K and $T = 300$ K are shown in Fig. 8, and are compared with the corresponding results predicted by the Marcus theory [41, 42]. As expected, at high (physiological) temperature the rate evaluated from the Marcus theory in a wide range of ε values agrees well with the rate evaluated from the spin-boson model at $T = 300$ K. However the Marcus theory and the spin-boson model differ significantly at $T = 10$ K. At such low temperature the rate as a function of ε for the spin-boson model is asymmetrical. This result agrees with observations reported in [65] which show a distinct asymmetry with respect to ε_M at low temperatures. Such asymmetry is not predicted by the models of Marcus and Hopfield [66–68].

If one makes the assumption that biological electron transfer systems evolved their ε values such that rates are optimized, one should expect that electron transfer rates in the photosynthetic reaction center are formed through a choice of $\varepsilon \to \varepsilon_{max}$, such that $k(\varepsilon_{max})$ is a maximum. In Fig. 9 the transfer rates $k(\varepsilon_{max})$ and $k(\varepsilon;T)$, corresponding for non-optimal values of $\varepsilon = \varepsilon_M \pm \delta$, with $\delta = 2.5$ kcal/mol, are shown. Experimental data of electron transfer processes in the photosynthetic reaction center show in-

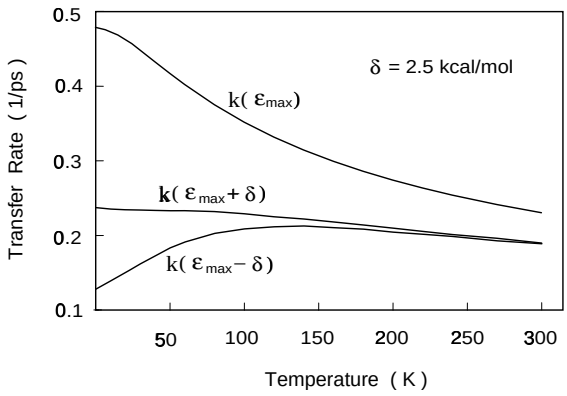

FIG. 9: Comparison of the temperature dependence of the maximum transfer rate of $k(\varepsilon_M)$ and off-maximum value $k(\varepsilon_{max} \pm \delta)$, where $\delta = 2.5$ kcal/mol. $k(\varepsilon_{max};T)$ represents the fastest transfer rate of the system, the rates $k(\varepsilon_{max} \pm \delta;T)$ are slower since their ε values deviate from the optimal value ε_{max}.

creases similarly to those presented in Fig. 9 [69–72]. However, Fig. 9 demonstrates also that electron transfer at ε values slightly off the maximum position can yield a different temperature dependence than that of $k(\varepsilon_M;T)$, namely temperature independence or a slight decrease of the rate with decreasing temperature. Such temperature dependence has also been observed for biological electron transfer [72]. The temperature dependence of the transfer rate resembles that of $k(\varepsilon_M;T)$ in photosynthetic reaction centers of native bacteria and in (M)Y210F-mutants with tyrosine at the 210 position of the M–unit replaced by phenylalanine. However, a replacement of this tyrosine by isoleucine [(M)Y210I-mutant] yields a transfer rate which decreases like $k(\varepsilon_M - \delta;T)$ shown in Fig. 9. This altered temperature dependence should be attributed to a shift of the redox potentials, i.e., $\varepsilon_M \rightarrow \varepsilon_M - \delta$.

It should be mentioned that there have been numerous similar investigations of biological electron transfer in the literature [73–76].

Acknowledgments

This work was supported in part by grants from the University of Missouri Research Board, the Institute for Theoretical Sciences (a joint institute of Notre Dame University and Argonne National Laboratory), the Department of Energy (Office of Science contract No. W-31-109-ENG-38), the National Science Foundation (FIBR-0526854) for I.K., and the National Institutes of Health (NIH 1-R01-GM067887-01) for K.S. Supercomputer time provided by the National Center for Supercomputing Applications (MCB020036) to

I.K. is also gratefully acknowledged.

---

[1] T. Renger, V. May, and O. Kuhn, Phys. Rep.-Rev. Sec. Phys. Lett. **343**, 138 (2001).

[2] V. Chernyak, W. M. Zhang, and S. Mukamel, J. Chem. Phys. **109**, 9587 (1998).

[3] V. May and O. Kühn, *Charge and Energy Transfer Dynamics in Molecular Systems* (WILEY-VCH, Berlin, 2000).

[4] S. Mukamel, *Principles of nonlinear optical spectroscopy* (Oxford University Press, New York, 1995).

[5] H. van Amerongen, L. Valkunas, and R. van Grondelle, *Photosynthetic Excitons* (World Scientific, Singapore, 2000).

[6] M. H. C. Koolhaas, G. van der Zwan, and R. van Grondelle, J. Phys. Chem. B **104**, 4489 (2000).

[7] A. Damjanovic, I. Kosztin, U. Kleinekathofer, and K. Schulten, Phys Rev E Stat Nonlin Soft Matter Phys **65**, 031919 (2002).

[8] L. Janosi, I. Kosztin, and A. Damjanovic, J. Chem. Phys. (2006).

[9] I. Mercer, I. Gould, and D. Klug, J. Phys. Chem. B **103**, 7720 (1999).

[10] J. Koepke, X. C. Hu, C. Muenke, K. Schulten, and H. Michel, Structure **4**, 581 (1996).

[11] G. McDermott, S. Prince, A. Freer, A. Hawthornthwaite-Lawless, M. Papiz, R. Cogdell, and N. Isaacs, Nature **374**, 517 (1995).

[12] L. M. P. Beekman, R. N. Frese, G. J. S. Fowler, R. Picorel, R. J. Cogdell, I. H. M. vanStokkum, C. N. Hunter, and R. vanGrondelle, J. Phys. Chem. B **101**, 7293 (1997).

[13] S. Georgakopoulou, R. N. Frese, E. Johnson, C. Koolhaas, R. J. Cogdell, R. van Grondelle, and G. van der Zwan, Biophys. J. **82**, 2184 (2002).

[14] X. Hu, T. Ritz, A. Damjanovic, F. Autenrieth, and K. Schulten, Q Rev Biophys **35**, 1 (2002).

[15] G. D. Scholes and G. R. Fleming, J. Phys. Chem. B **104**, 1854 (2000).

[16] O. J. G. Somsen, R. vanGrondelle, and H. vanAmerongen, Biophys. J. **71**, 1934 (1996).

[17] V. Sundstrom, T. Pullerits, and R. van Grondelle, J. Phys. Chem. B **103**, 2327 (1999).

[18] H. M. Wu, M. Ratsep, R. Jankowiak, R. J. Cogdell, and G. J. Small, J. Phys. Chem. B **101**, 7641 (1997).

[19] M. Yang, R. Agarwal, and G. R. Fleming, J. Photochem. Photobiol. A-Chem. **142**, 107 (2001).

[20] Z. He, V. Sundstrom, and T. Pullerits, J. Phys. Chem. B **106**, 11606 (2002).

[21] X. Hu, A. Damjanovic, T. Ritz, and K. Schulten, Proc. Natl. Acad. Sci. USA **95**, 5935 (1998).

[22] J. A. Ihalainen, J. Linnanto, P. Myllyperkio, I. H. M. van Stokkum, B. Ucker, H. Scheer, and J. E. I. Korppi-Tommola, J. Phys. Chem. B **105**, 9849 (2001).

[23] S. J. Jang and R. J. Silbey, J. Chem. Phys. **118**, 9324 (2003).

[24] J. Linnanto, J. E. I. Korppi-Tommopa, and V. M. Helenius, J. Phys. Chem. B **103**, 8739 (1999).

[25] T. Meier, Y. Zhao, V. Chernyak, and S. Mukamel, J. Chem. Phys. **107**, 3876 (1997).

[26] J. Ray and N. Makri, J. Phys. Chem. A **103**, 9417 (1999).

[27] X. Hu, A. Damjanović, T. Ritz, and K. Schulten, Proc. Natl. Acad. Sci. USA **95**, 5935 (1998).

[28] X. Hu and K. Schulten, Physics Today **50**, 28 (1997).

[29] W. Humphrey, A. Dalke, and K. Schulten, J. Mol. Graphics **14**, 33 (1996).

[30] J.-P. Zhang, R. Fujii, P. Qian, T. Inaba, T. Mizoguchi, and Y. Koyama, J. Phys. Chem. B **104**, 3683 (2000).

[31] V. May and O. Kühn, *Charge and Energy Transfer Dynamics in Molecular Systems* (WILEY-VCH, Berlin, 2000).

[32] G. D. Mahan, *Many-Particle Physics* (Plenum Press, New York, 1990), 2nd ed.

[33] S. Mukamel, *Principles of Nonlinear Optical Spectroscopy* (Oxford University Press, New York, 1995).

[34] N. Makri, J. Phys. Chem. B **103**, 2823 (1999).

[35] K. Schulten and M. Tesch, Chem. Phys. **158**, 421 (1991).

[36] S. A. Egorov, K. F. Everitt, and J. L. Skinner, J. Phys. Chem. A **103**, 9494 (1999).

[37] T. Holstein, Ann. Phys.(N.Y.) **8**, 343 (1959).

[38] D. Xu and K. Schulten, Chem. Phys. **182**, 91 (1994).

[39] H. v. Amerongen, L. Valkunas, and R. v. Grondelle (2000).

[40] J. Deisenhofer, O. Epp, K. Mikki, R. Huber, and H. Michel, Nature **318**, 618 (1985).

[41] R. A. Marcus, J. Chem. Phys. **24**, 979 (1956).

[42] R. A. Marcus, J. Chem. Phys. **24**, 966 (1956).

[43] A. J. Leggett, S. Chakravarty, A. T. Dorsey, M. P. A. Fisher, A. Garg, and W. Zwerger, Rev. Mod. Phys. **59**, 1 (1985).

[44] A. D. MacKerell Jr., D. Bashford, M. Bellott, et al., FASEB J. **6**, A143 (1992).

[45] A. D. MacKerell Jr., D. Bashford, M. Bellott, et al., J. Phys. Chem. B **102**, 3586 (1998).

[46] M. Schlenkrich, J. Brickmann, A. D. MacKerell Jr., and M. Karplus, in *Biological Membranes: A Molecular Perspective from Computation and Experiment*, edited by K. M. Merz and B. Roux (Birkhauser, Boston, 1996), pp. 31–81.

[47] W. L. Jorgensen, J. Chandrasekhar, J. D. Madura, R. W. Impey, and M. L. Klein, J. Chem. Phys. **79**, 926 (1983).

[48] M. N. Ringnalda, J.-M. Langlois, R. B. Murphy, B. H. Greeley, C. Cortis, T. V. Russo, B. Marten, R. E. D. Jr., W. T. Pollard, Y. Cao, et al., *PS-GVB v2.3*, Schrödinger Inc., Portland, OR (1996).

[49] N. Foloppe, J. Breton, and J. C. Smith, in *The Photosynthetic Bacterial Reaction Center II: Structure, Spectroscopy and Dynamics*, edited by J. Breton and A. Vermeglio (Plenum Press, New York and London, 1992), pp. 43–48.

[50] N. Foloppe, M. Ferrand, J. Breton, and J. C. Smith, PROTEINS: Structure, Function, and Genetics **22**, 226 (1995).

[51] MSI, *QUANTA 97*, Molecular Simulations Inc., Burlington, Massachusetts (1997).

[52] S. E. Feller, Y. H. Zhang, R. W. Pastor, and B. R. Brooks, J. Chem. Phys. **103**, 4613 (1995).

[53] T. Darden, D. York, and L. Pedersen, J. Chem. Phys. **98**, 10089 (1993).

[54] J. C. Phillips, R. Braun, W. Wang, J. Gumbart, E. Tajkhorshid, E. Villa, C. Chipot, R. D. Skeel, L. Kale, and K. Schulten, J. Comput. Chem. **26**, 1781 (2005).

[55] S. Miyamoto and P. A. Kollman, J. Comp. Chem. **13**, 952 (1992).

[56] M. G. Cory, M. C. Zerner, X. Hu, and K. Schulten, J. Phys. Chem. B **102**, 7640 (1998).

[57] J. Ridley and M. Zerner, Theor. Chim. Acta **32**, 111 (1973).

[58] M. Zerner, G. Loew, R. Kirchner, and U. J. Mueller-Westerhoff, Am. Chem. Soc. **102**, 589 (1980).

[59] A. Damjanovic, H. M. Vaswani, P. Fromme, and G. R. Fleming, J. Phys. Chem. B **106**, 10251 (2002).

[60] J. Linnanto and J. Korppi-Tommola, J. Comput. Chem. **25**, 123 (2004).

[61] HyperChem(TM), Hypercube, Inc., 1115 NW 4th Street, Gainesville, Florida 32601, USA.

[62] M. J. Frisch, G. W. Trucks, H. B. Schlegel, G. E. Scuseria, M. A. Robb, J. R. Cheeseman, J. A. M. V. G. Zakrzewski, R. E. Stratmann, J. C. Burant, J. M. M. S. Dapprich, et al., *Gaussian 98*, Gaussian Inc., Pittsburgh, PA (1998).

[63] K. Visscher, H. Bergstrom, V. Sundström, C. Hunter, and R. van Grondelle, Photosynth. Res. **22**, 211 (1989).

[64] D. Xu and K. Schulten, in *The Photosynthetic Bacterial Reaction Center: II. Structure, Spectroscopy and Dynamics*, edited by J. Breton and A. Vermeglio (Plenum Press, New York, 1992), NATO ASI Series A: Life Sciences, pp. 301–312.

[65] J. R. Gunn and K. A. Dawson, J. Chem. Phys. **91**, 6393 (1989).

[66] J. J. Hopfield, Proc. Natl. Acad. Sci. USA **71**, 3640 (1974).

[67] R. A. Marcus and N. Sutin, Biochim. Biophys. Acta **811**, 265 (1985).

[68] H. Sumi and R. A. Marcus, J. Chem. Phys. **84**, 4894 (1986).

[69] M. Bixon and J. Jortner, J. Phys. Chem. **90**, 3795 (1986).

[70] C. Kirmaier and D. Holten, in *The Photosynthetic Bacterial Reaction Center: Structure and Dynamics*, edited by J. Breton and A. Vermeglio (Plenum Press, New York and London, 1988), pp. 219–228.

[71] J. L. Martin, J. Breton, J. C. Lambry, and G. Fleming, in *The Photosynthetic Bacterial Reaction Center: Structure and Dynamics*, edited by J. Breton and A. Vermeglio (Plenum Press, New York and London, 1988), pp. 195–203.

[72] V. Nagarajan, W. W. Parson, D. Gaul, and C. Schenck, Proc. Natl. Acad. Sci. USA **87**, 7888 (1990).

[73] A. Warshel, Z. T. Chu, and W. W. Parson, Science **246**, 112 (1989).

[74] A. Warshel and J.-K. Hwang, J. Chem. Phys. **84**, 4938 (1986).

[75] P. G. Wolynes, J. Chem. Phys. **86**, 1957 (1987).

[76] C. Zheng, J. A. McCammon, and P. G. Wolynes, Proc. Natl. Acad. Sci. USA **86**, 6441 (1989).